Analysis of small-scale sediment changes to an underdeveloped sand dune

To be turned in on November 20th, 2015 to Dr. Mark Besonen for Geol 3442.

Report written and prepared by Angelo Marney

Abstract:
A study was conducted to measure the short-term change in sediment across the face of an underdeveloped dune; the dune was located just off of Newport Pass Road and had geospatial coordinates N27°37'51.49", W97°11'42.32". Two sets of approximately 120 overlapping photos were taken with a cell phone camera of a region on the backside of the dune on 7 November 2015 and on 12 November 2015. These two sets of photos were inputted into an algorithm known as Structure from Motion to yield two 3-D point-clouds which represented the surface of the photographed regions at the time of photo acquisition. These two point-clouds were then aligned based on cloud similarity using free software CloudCompare, and were then exported as raster digital elevation models into qGIS, where they were further aligned and scaled according to on-site measurements and geospatial coordinates. The digital elevation models were then differenced and analyzed to determine the change in sediment transport over certain regions of the dune. Over the brief period of time between photo acquisitions, the dune accumulated sediment (on the scale of millimeters) in its northernmost and southernmost regions. Sediment was lost from the relative center and westernmost regions. The positions of the regions where sediment accumulation occurred corresponded to the overall dominant wind directions over the brief period between photo acquisitions when taking minimum entrainment velocity into account. Micro-topographic factors and nearby vegetation were also taken into consideration to enhance interpretation. The results of this study are consistent with the principles of dune migration, and shed light on how standard wind conditions over brief periods of time affect dunes on very small scales.

Introduction:
The most important force that forms and affects dunes is wind. Wind acts as a constant force that is often strong enough to entrain and transport sand-sized particles over short distances via the process of saltation. In this saltation process, sand-sized grains are lifted off the ground by wind and are transported short distances before landing and striking other sand grains; this grain-to-grain collision leads to a transfer in kinetic energy which causes struck particles to lift off the ground and be transported by wind, resulting in further saltation. The sand-sized grains that compose coastal dunes are usually too massive to be suspended by normal wind conditions, so it is unlikely that suspension plays a significant role in short-term migration during normal conditions. Wind acting on dunes can also nudge particles along the surface of the dune causing gravity-driven surface grain flows. These surface grain flows, along with sediment transport downwind due to saltation, are likely the leading causes of long term and short term dune migration.

Vegetation is also an extremely important factor that greatly affects dune morphology by allowing dunes to mature and stabilize. Vegetation allows for dune stabilization by acting as a

natural barrier to slow down the flow of wind, decreasing its potential to push and pick up surrounding grains. Vegetation also has the tendency to anchor itself into the sand and trap windblown grains landing near it, causing sediment accumulation to sometimes occur. Dunes which are heavily covered by vegetation tend to be more mature and stable than dunes with low vegetation cover. For partly this reason, the data that was collected for this study involved a region of a dune with very low amounts of vegetation cover, as it was expected that an underdeveloped and less-stable dune would exhibit more sediment change over a brief time period under ordinary wind conditions.

In order to analyze the chosen dune, an algorithm known as Structure from Motion (SfM) was put to use. SfM is an algorithm that takes in a set of overlapping photos of an object or region, and outputs a sparse point-cloud roughly representing the surface of the photographed object or region by matching points on the set of overlapping photos to each other. SfM offers a low-cost way of quickly creating an accurate model of both large scale and small scale regions and has great potential to be used in geomorphology; a general workflow for the usage of SfM for geomorphic applications is outlined in certain scientific papers (e.g., Westoby et al., 2012).

By generating two 3-D point-cloud of the surface of the dune at different times, one should theoretically be able to project the two point-clouds as digital elevation models (DEMs), and subtract these two DEMs to get an estimation of the amount of sediment change over the modeled region between the times of photo acquisition. It was crucial that vegetation cover was sparse so that DEM differencing would provide true sediment changes rather than vegetation-position changes. The alignment of the two point-clouds and further alignment and scaling of the DEMs was crucial in the analysis. The first set of photos used to generate the first point-cloud were taken on 7 November 2015 and the second set of photos used generate the second point-cloud were taken on 12 November 2015. The chosen region to be photographed was that of back-side of an underdeveloped sand dune that was located near to Newport Pass Road; it had geospatial coordinates N 27°37'51.49", W 97°11'42.32". After necessary alignment, projection, and differencing, statistical elevation change data was extracted and analyzed in conjunction with local wind data (obtained from timeanddate.com) and topographic characteristics of the model.

Methods:

On 7 November 2015, six markers were wedged into the dune at sufficiently spaced distances in order to aid in the point-cloud registration. Approximately 130 photographs were taken at different converging angles and heights were obtained using a smart-phone camera and a ladder. After photo acquisition, four of the markers were removed with extreme care so as not to disturb the dune; two markers were left buried within the dune. On 12 November 2015, the site was returned to take a second set of around 140 photos with the same camera. The straight-line

distance between two highly distinguishable vegetation patches were recorded with a tape measure, and the geospatial coordinates of these patches were also recorded. A very rough distance between the lowest points to be modelled to the highest points to be modelled was recorded using a tape measure. The two sets of photos were analyzed on a computer and blurry were removed, resulting in 119 remaining photos from the first day and 123 photos from the second day.

The two batches of photos were then imported into AgiSoft Photoscan, where two sparse 3-D point-cloud were generated. Both point-clouds were then densified and then imported into CloudCompare, where they were simultaneously displayed and manually rotated/scaled so that they roughly aligned with each other. Once the two point-clouds were roughly aligned/scaled to match each other, a tool was used to further automatically align and scale the point-clouds based on manually-selected matching points on each cloud. Once the point-clouds were aligned, they were rotated together to establish a common base-level. The two point-clouds were then exported as raster files with identical step-sizes; the values of the raster tiles corresponded to the minimum height of the cloud in the tile. These two raster/DEMs were then imported into free software qGIS and were further aligned using raster tools.

The next step was to establish real-world scales for the DEMs, as the obtained GPS coordinates failed to establish an accurate scale. First, a GPS-obtained decimal degree coordinate of a point was attached to one of the DEMs using the georeferencer tool. Next, using a measurement tool in CloudCompare, the straight-line distance, and horizontal x & y distances in unitless point-cloud values between this georeferenced point and a second point was obtained. From the unitless straight-line distance and measured distance in meters, a conversion factor between unitless point-cloud distance and real-world meters was generated, which was used to establish the horizontal x & y distances between the two points in meters. A conversion factor between decimal degrees and meters was then found by taking into account latitude, and this conversion factor was used to convert the x & y distances in meters into x & y decimal degree distances. The new decimal degree distances were then subtracted from longitude and latitude coordinates to yield new geospatial coordinates, which were then attached to the corresponding point using the georeferencer tool. Running a profile tool across the second DEM and differencing the max and min points yielded a unitless height value, which was compared to the estimated real-world height value to obtain a rough conversion factor between unitless DEM height and meter height. With these two geospatial coordinates, the DEMs were scaled.

Using the raster calculator tool in qGIS, the first DEM was subtracted from the second DEM to produce a differenced-raster which contained values corresponding to the difference in height values between the two DEMs. Two regionally-divided polygon shapefiles were created (avoiding vegetation). Using a zonal statistics tool, statistical values from the differenced-raster

were exported into excel and were separated based on the regional divisions. Wind data that was generated in six hour intervals over the study period was obtained from online archives (timeanddate.com) to be used in the analysis.

Results:

Figure 1 is a plot containing the average changes in elevation between the dates of photo acquisition. The A1 through A14 values are qualitative values corresponding to specific zones separated based on how far north and how far south the zones were located. A-values closer to 1 correspond to zones that were located farther north, while A-values closer to 14 correspond to zones that were located farther south. A visualization showing how the polygonised region was divided into A-zones is shown in figure 2. A consistent straight-line spacing of 1.071 m was set between the boundaries of each region, so there was a distance of approximately 12.852 m from the southern border of the northernmost region to the northern border of the southernmost region. The area contained within these A-zones was highly variable, with the largest zone having an area of approximately 3.93 m^2, and the smallest zone having an area of approximately 0.27 m^2.

In zones A1, A5, A6, A7, A8, A13, and A14 there was a decrease in average elevation between the times of photo acquisition; the exact numerical values of these elevation changes can be seen in table 1. In these zones of negative elevation change, the total average elevation change was negative 37.2 mm. It is worthy to note that zones A1 and A12 experienced elevation loss that was far below average. In zones A2, A3, A4, A9, A10, and A11, there was an overall increase in average elevation between the times of photo acquisition; the exact numerical values of these elevation changes can also be seen in table 1. Ranging within these zones of positive elevation change, the total average elevation change was positive 29.3 mm. It is worthy to note that zone A9 had experienced elevation gain that was far below average. Zones of negative elevation change covered approximately 52.4% of the polygonized area (approximately 16.68 m^2) while zones of positive elevation change covered approximately 47.6% of the polygonized area (approximately 15.14 m^2).

Figure 3 is a plot containing average changes in elevation between the dates of photo acquisitions. This time, the B1 through B11 parameters are qualitative values that correspond to zones separated based on eastward and westward location, with B-values closer to 1 corresponding to zones that were located further west, and B-values closer to 11 corresponding to zones that were located further east. An image showing B-zones division is shown in figure 4. The same consistent straight-line spacing of 1.081 m was used, resulting in a distance of approximately 9.639 m from the western border of the easternmost zone to the eastern border of the westernmost zone. The area contained within these B-regions were highly variable, with the largest zone having an area of approximately 4.864 m^2, and the smallest zone having an area of approximately 0.632 m^2.

In regions B1, B2, B3, B4, B5, B6, B7, B10 and B11, there was a decrease in average elevation between the times of photo acquisition; the exact numerical values of these elevation changes can be seen in table 2. Ranging within these zones of negative elevation change, the total average elevation change was negative 9 mm. In zones B8 and B9, there was an overall increase in average elevation between the times of photo acquisition; the exact numerical values of these elevation changes can also be seen in table 2. In these zones of positive elevation change, the total average elevation change was positive 18.2 mm. Zones of negative elevation change covered approximately 81.5% of the polygonised area (approximately 26.93 m^2) while zones of positive elevation change covered approximately 18.5% of the polygonised area (approximately 6.13 m^2). The total average elevation change for the entire polygonised region of the dune was negative 4.2 mm. Area values for analysis on A-zones and B-zones do not add up to the same value, this is because small sub-zones with miniscule areas were ignored in both cases. Multiplying polygonised area by total average elevation change yields a total sediment volume loss of 138 mm^3 (shown in table 3).

Figure 5 contains a wind-rose plot for Corpus Christi from data which was updated in 6 hour intervals over the time period from 7 November to 12 November. Data for this wind-rose plot was obtained from an online website with wind archive information (timeanddate.com). The total average wind over this time period can be represented as a vector, with a magnitude (velocity) of 2.165 (m/s) pointing 238.15 degrees from north (west-south-west); this average wind was obtained using the principles of polar coordinate conversion and vector addition. Figure 6 is an image showcasing the first point cloud. Figure 7 is an image showcasing the first DEM, and figure 8 showcases the second DEM. Figure 9 showcases the differenced-raster from which data values were obtained. Table 3 gives the total average elevation change and average volumetric change as well as the total average wind magnitude and direction. These extra figures and tables are to be used in the interpretation.

Interpretation:

The major assumption made in the following analysis is given by the differenced raster corresponds to the change in sediment amount over the region of overlap. Figure 1 shows that, on average, the northern and southern zones of the modeled region experienced a larger amount of sediment accumulation along with a smaller amount of sediment removal when compared to other regions. This can be visualized in figure 2 by looking at the positions of the zones of significant sediment accumulation, specifically zones A2, A3, A4, A10, and A11. Zones A1 and A12 both showed sediment loss despite being on the southern and northern ends of the region, but the sediment loss in these two regions was much lower than the average sediment loss in areas where there was an overall decrease in sediment. The insignificance in the amount of

sediment loss in the northern zone A1 and southern zone A12 further supports the interpretation that sediment accumulation was focused on the northern and southern regions of the dune.

It can also be seen in figures 1 and 2, that zones located near the center of the modeled region, such as zones A5, A6, A7, and A8, experienced a larger amount of average sediment removal than sediment accumulation. Zone A9 has a positive elevation change value despite being located near the center of the modeled region, but analysis of the figure shows that zone A9 had an average sediment change that was much lower than total average sediment change when compared to the zones of sediment accumulation. The fact that zone A9 experienced a fairly insignificant amount of positive elevation change further supports the interpretation that zones located around the center were zones of sediment removal rather than zones of sediment accumulation. The only region that does not fit this interpretation is region A14, but this may be insignificant as it was the smallest region modeled with an area of merely 268 mm^3. A look at figure 9 also reveals brightly-colored bands representing areas of sediment deposition in both the southern and northern regions of the modeled region, as well as a large dark region representing areas of sediment loss can be seen between these two bright bands, which further lends support to these interpretations of the data.

Figure 3 shows that, on average, an insignificant portion of the eastern zones of the modeled region experienced an increased amount of sediment over the periods between photo acquisitions. This is visualized within figure 4 by looking at the positions of the zones of significant sediment accumulation, specifically zones B8 and B9. This initial interpretation is not supported by zone B11. Zone B10 contained also contained sediment loss, though this amount may be negligible. The fact that only two zones experienced accumulation on the entire eastern side of the region is a cause for concern that should make one question the results of the data. There is a decent chance that the trend supporting this interpretation was generated (or enhanced) by errors occurring in the creation of the second point cloud (or during the process of digital elevation model differencing), as the differenced raster shown in figure 9 contains very small bright spots around the center of where zones B8 and B9 cover. Such an error would originally stem from poor photo acquisition techniques, most likely not using the proper geometrical image-acquisition techniques. These error-induced bright spots are fairly small yet are significantly bright, but they are not the only areas with above average elevation in zones B8 and B9, so while it is certain that these bright points skew the elevation to support eastward accumulation, it is still possible (yet unlikely) that the trend would still exist without these sources of error (if these trends existed without such errors, they would at the very least be much less prominent than what is currently shown in the data). As visualized in figures 3 and 4, zones located on the western and center regions of the polygonised model, such as zones B1, B2, B3,

B4, B5, B6, and B7, experienced a larger amount of average sediment removal than sediment accumulation.

When taking the wind data (from timeanddate.com) into account, a potential explanation is provided for some of the trends supporting the interpretations made previously. Looking at figure 5 and the average wind direction in data table 3, it can be clearly seen that wind blew towards the west and south the most. During some days, there was a significant wind blowing from 8 to 10 m/s towards the north, and the components of north-blowing wind canceled with the components of the south blowing wind during the calculation of overall average wind direction, yielding a wind direction blowing towards west-south-west with magnitude 2.17 m/s. This overall average wind direction being west-south-west does not provide good evidence to justify or refute any of our interpretations, namely that wind direction over short periods of time acts as a good indication of expected regions of sediment deposition and removal. In order to get a better idea of what is happening, it is necessary to look at figure 5 as well as the micro-topographic features visible in figures 5, 6, 7, and 8. For example, this overall average wind direction might lead one to believe that sediment should have only accumulated in the southern and western regions and not in the northern region, but this was not the case. It is plausible that the fast north blowing winds pushed sediment across the central region of the dune and deposited them right over the northern hill slope that is easily visible in figures 7 and 8. The small vegetation patch around this northern region of deposition may have also aided in these accumulation related processes by slowing down the wind in this small region causing it to lose its ability to transport sediment, and likely acted as a sediment trap to promote further accumulation in nearby areas. Despite wind direction being by far the prominent factor affecting dune morphology, it is still useful to look for other factors that may provide additional explanation.

One surprising result that can be seen in the figure 5 and figure 3 is that, despite winds hardly blowing towards the east, some sediment accumulation appeared to occur in the eastern zones of the modeled dune. Winds that blew predominantly western were of very high occurrence but generally had low average of wind speeds ranging from 2 to 4 m/s, which may not have been strong enough for significant saltation to occur. Sediment transport from such weak winds would be severely limited, which explains the overall smaller range of sediment change in seen in figure 3 and table 2 compared to figure 1 and table 1. It is possible that eastern sediment accumulation that occurred in zones B8 and B9 could be attributed to the local topographic positions of these regions, as figures 7 and 8 show that these zones contained significant areas located at the bases of higher elevation regions (where gravity might promote sediment accumulation). In addition to these possible explanations, it cannot be forgotten that there are definitely errors in the differenced raster from which all statistical analysis was done, as

can be seen in the bright spots skewing sediment accumulation upwards in figure 9. Since there was low western wind speeds, low elevation areas within western accumulation zones B8 and B9, and error-induced bright spots promoting sediment increase values in zones B8 and B9, it is likely the case that the apparent initial trend of sediment accumulating upwind in the eastern regions despite the lack of east blowing wind is not be a reliable interpretation to be made from the data.

One final interpretation that can be made is that over the brief period of time, dunes with low amounts of vegetation experience an overall loss of sediment due to these dunes being less stable and thus easier to erode. The section of the dune studied in this experiment was extremely bare, with only four visible vegetation patches in the modeled region. This lack of vegetation leaves sediments exposed and easy to erode away. This is seen in data table 5, as the overall estimated volumetric sediment loss for the modeled region was approximately 137.6 mm^3.

Discussion:

This study provided insight into how wind-driven processes affect coastal dunes on very small scales and in very short time frames. Many of the major concepts and processes that were important to this study were mentioned in lecture as well as in the Forman et al. 2009 article. In particular, the concepts of dune stabilization via vegetation cover, of minimum wind entrainment velocity, and of dune migrations occurring in the overall average wind direction were of great importance for this analysis. It was seen that relationships could be established between wind direction and sediment transport over the course of just a few days, provided that wind speed was sufficiently high and provided that sediment transport could be analyzed on millimeter scales. This daily millimeter change in sediment may not be significant when looking at a single dune, but if one were to look at an entire coastal dune system, the sheer volume of sediment transported by wind-driven processes on windy days must be enormous. These wind-driven erosive processes dominate arid landscapes and one can only imagine how often desert sands shift over short periods of time.

The fact that sand-sized grains dominate coastal dune landscapes leads one to believe that saltation is the dominant processes by which sediment is transported by wind, and is thus a dominant process affecting and shaping coastal sand dunes. Lower wind speeds lack the energy needed to entrain these coastal sand grains, and it is expected that these lower wind speeds would cause sand-grains to be transported a relatively small distance when compared to winds with high-energy high-velocity winds. Due to this fact, further studies involving sediment change over small periods of time should take the local wind conditions over the study period into great consideration. The idea that wind direction corresponds to direction of sediment erosion is supported by the results of the study by the fact that high wind velocities occurred in the northern

and south directions, and it was the northern and southern regions of the modeled region where sediment accumulation occurred.

Sediment accumulation in the northern and eastern regions also showed the importance of not interpreting the scientific results one dimensionally. In order to get a reasonable explanation for the accumulation of sediment in northern and eastern regions, micro-topographic factors involving surrounding heights as well as nearby vegetation patches needed to be taken into account as to come up with plausible explanations for increased deposition rates in regions where sediment loss might be expected. The eastern region of accumulation in particular also showed the importance of considering the possibility of errors in the statistical data due discontinuity points in the generated model. The lack of sediment deposition in the western region despite prominent westerly directed winds is likely due to the fact that that westerly winds were, for the most part, within the two to four meter per second wind range, which is likely not high enough to support sand-grain entrainment.

The chosen dune region was very underdeveloped and was located right next to a common beach access road. The fact that this dune was located next to such an access road and had such low vegetation cover suggests that it was established fairly recently. Inputting the coordinates of the study site into Google Earth shows tire tracks covering the dune; the only present material that appears to be supporting sand accumulation looks like some sort of washed up sea-grass material. Just outside of the modeled region, man-made materials and garbage is visibly buried on the other side of the dune (facing the shoreline). This man-made material may also have contributed the further development of the dune, as vegetation cover for this dune was very sparse and would not have been sufficient in establishing the dune (the dune looked nothing like commonly-seen heavily-vegetated coppice dunes which were abundant in locations near the chosen study site). The overall lack of vegetation greatly lessened the stability of the dune; it is worthy to note that, in the Forman et al. 2009 article, vegetation cover was the first order factor determining whether or not sediment removal would occur, with all other contributing factors being directly related to how they affect vegetation cover. This lack of dune stability due to low vegetation cover is shown by the overall loss of volumetric sediment grains in the modeled region. It is still possible that this sea-grass/man-made started dune will grow slightly over the next few years, but it is much more likely that sediments making up the dune will continually be eroded away, causing the dune to migrate and possibly merge with the more stable dunes in the surrounding region.

In addition to providing insight into dune formation and Eolian processes, this study shows how SfM may be used to model small scale geomorphic features. SfM is a very low cost and easy to use and it has the potential to be applied to many geologic projects, from the quantification of some sediment change, to the mapping of large scale regions. SfM may also

potentially be used to generate models of interesting geomorphic features to be used in classroom settings, as data acquisition is relatively simple and actual meshes and surface reconstructions can be created for visualization purposes if one so desires. One of the main concerns with this approach to modeling/mapping is that the modeled region must be relatively vegetation, as there is no way to get accurate elevation data for regions covered by vegetation. Care must be taken when acquiring photos as the geometric relationship between the photographed region and the cameras is extremely important in order to get a model without serious holes in it. This analysis project was also a nice first exposure to GIS software, which may be used for further personal research projects.

Conclusion:

Using photos taken with a cell-phone camera, the Structure from Motion algorithm was used to generate two accurate 3-D point-clouds of a region of a sand dune located just off of Newport Pass Road at geospatial coordinates N27°37'51.49", W97°11'42.32". These “before and after” point-clouds were further processed in CloudCompare and qGIS to get the clouds precisely aligned. A real world scale was implemented using geospatial coordinate data and the rasters generated in CloudCompare were differenced in qGIS. This differenced raster contained data values corresponding to the difference in elevation between the photographed dune between the times of photo acquisition, and the qGIS zonal statistics tool were used to extract statistical information about this differenced raster. It was found that the dunes accumulated sediment in regions corresponding to that of predominant wind direction when assuming a minimum entrainment velocity of 6 m/s. The modeled region saw an overall decrease in sediment as there was very little vegetation covering the dune. It can be expected that this dune will migrate through the years in the direction of dominant wind unless vegetation cover is established. Many of the concepts learned in lecture about wind-driven processes was applied in the analysis of the data.

Appendix:

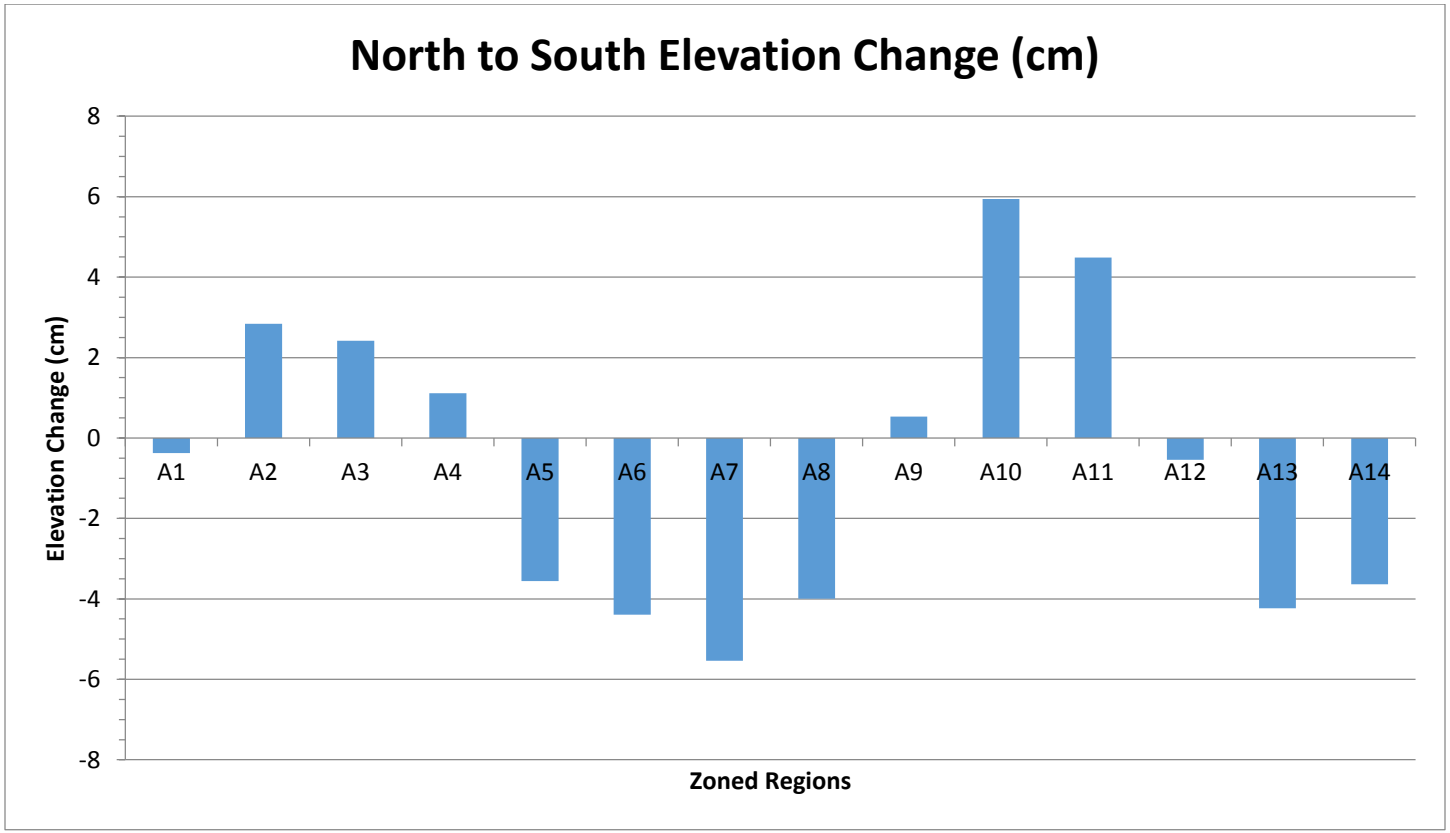

Figure 1. On the vertical axis, the difference in the elevation values between the dates of photo acquisition are given in centimeters, the exact values were derived from the qGIS zonal statistics tool and are listed in table 1. The minor tick marks along the vertical axis correspond to a half-centimeter interval. On the horizontal axis, the "A values" correspond to regions separated and ordered based on relative northerly and southerly positions, with zones closer to A1 being more northerly while zones closer to A14 being more southerly. It is necessary to see figure 2 to visualize the positions of these regions to better appreciate this plot. There were positive changes in elevation in the northern zones A2, A3, & A4, as well as in the southern zones A9, A10, & A11. Northern zone A1 and southern zone A12 experienced a negligible amount of sediment decrease, so they do not hurt the apparent trend a significant amount. Zones of negative elevation changes were typically located in the center, as exhibited by A5, A6, A7, & A8. Central-southern zone A9 has a negligible amount of sediment increase, so it does not take away much from the apparent trend. The range of this figure is larger than that of the range of figure 4.

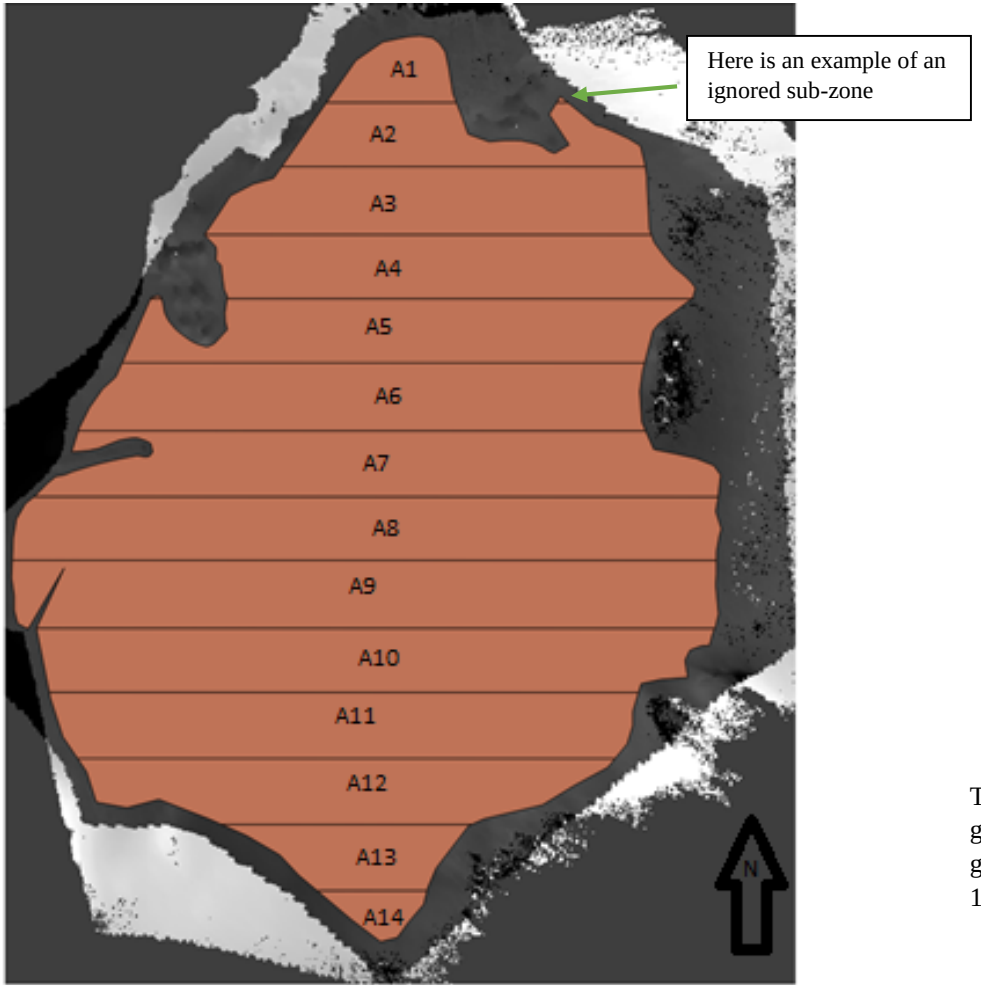

Figure 2: An image showing A-zone division. To be utilized as a supplement to figure 1. A consistent straight-line spacing of 1.071 m was set between the boundaries of each region border of the southernmost region. The area contained within these A-zones was highly variable, with the largest zone having an area of approximately 3.93 m^2, and the smallest zone having an area of approximately 0.27 m^2.

Zone Value	Average Height Change (mm)	Area (m^2)
A1	-3.7	0.52
A2	28.4	1.32
A3	24.2	2.32
A4	11.1	2.40
A5	-35.5	2.58
A6	-43.9	3.03
A7	-55.4	3.34
A8	-39.9	3.69
A9	5.3	3.93
A10	59.5	3.38
A11	44.9	3.13
A12	-5.5	2.34
A13	-42.3	0.93
A14	-36.3	0.27

Table 1: The precise values of elevation change in meters given over the appropriate A-zone. Area of A-zones are given in squared meters. These values correspond to figures 1 and 2.

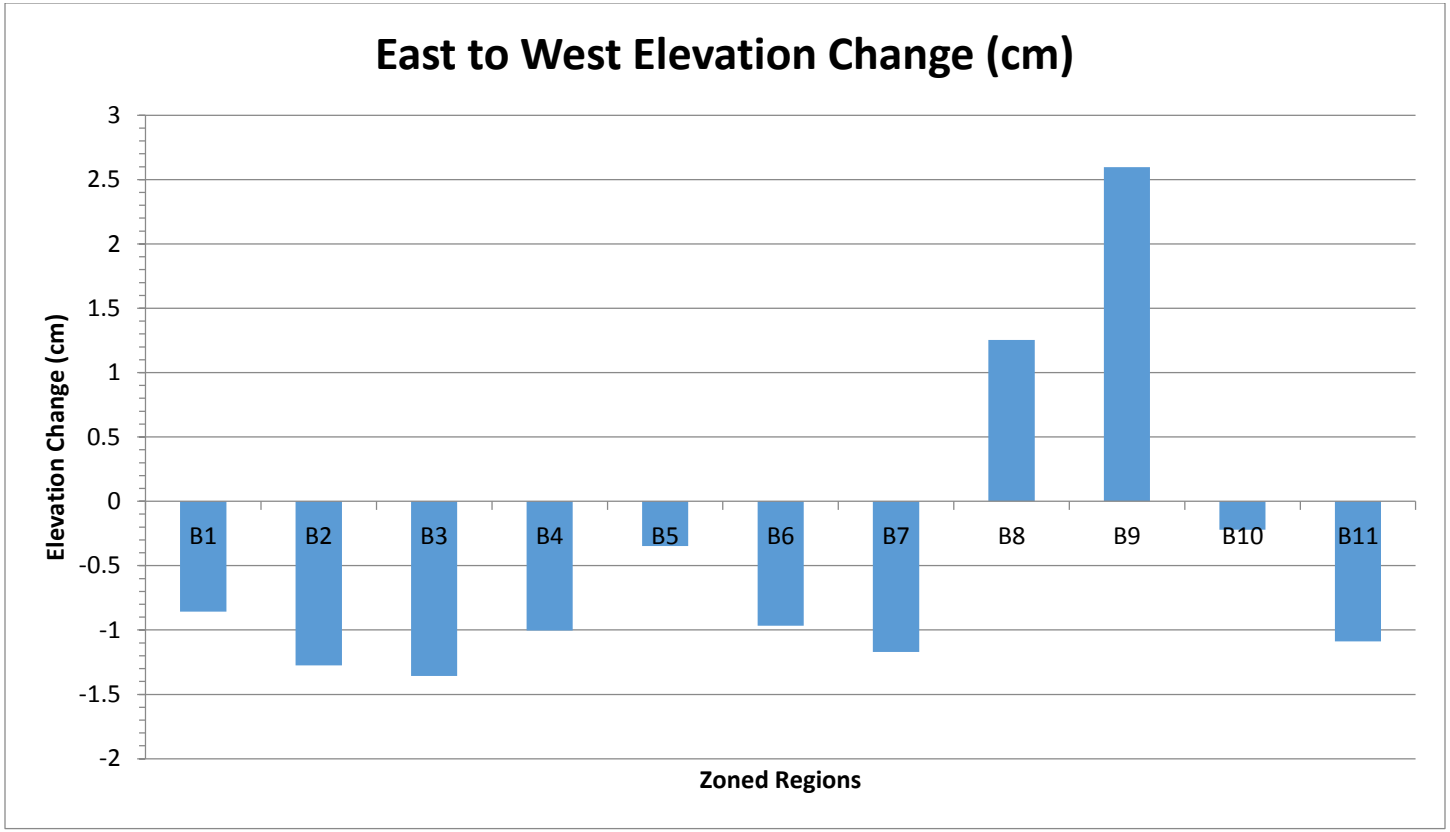

Figure 3. On the vertical axis, the difference in the elevation values between the dates of photo acquisition are given in centimeters, the exact values were derived from the qGIS zonal statistics tool and are listed in table 2. The minor tick marks along the vertical axis correspond to a 0.1 centimeter interval. On the horizontal axis, the "B values" correspond to regions separated and ordered based on relative easterly and westerly positions, with zones closer to B1 being more westerly while zones closer to B14 being more easterly. It is necessary to see figure 4 to visualize the positions of these regions to better appreciate this plot. There were positive changes in elevation in the eastern zones B8 & B9. Zones of negative elevation changes were typically located in around western region and near the center, as exhibited by zones B1, B2, B3, B4, B5, B6, & B7. Zones B10 and B11 showed negative sediment accumulation despite being located on the eastern side of the region. The range of this figure is significantly smaller than that of the range of figure 1, suggesting that eastern/western sediment transport was less prominent than northern/southern sediment transport. It is likely that the high sediment accumulation in region B8 and B9 are due to errors in cloud generation, this is explained in the interpretation section and is supported by random bright spots in figure 9.

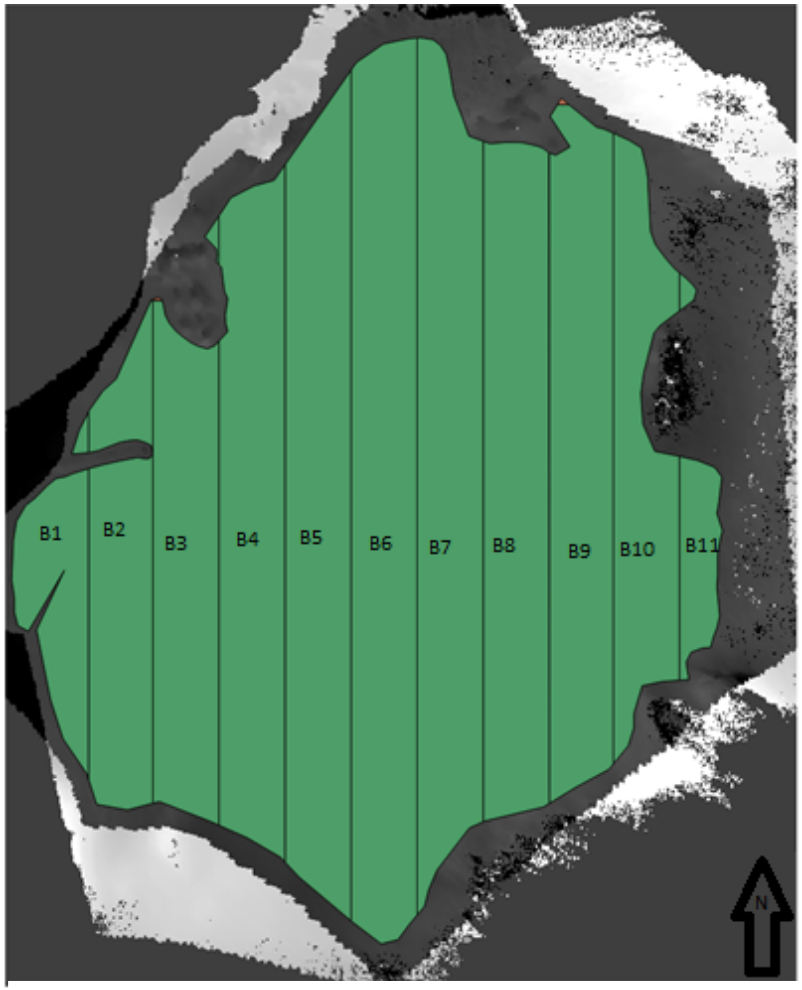

An image showing B-zone division. To be utilized as a supplement to figure 3. A consistent straight-line spacing of 1.071 m was set between the boundaries of each region border of the southernmost region. The area contained within these B-zones was highly variable, with the largest zone having an area of approximately 4.864 m^2, and the smallest zone having an area of approximately 0.632 m^2.

Zone Value	Average Height Change (mm)	Area (m^2)
B1	-8.6	0.63
B2	-12.8	2.40
B3	-13.6	3.48
B4	-10.0	3.68
B5	-3.5	4.17
B6	-9.7	4.87
B7	-11.7	4.14
B8	125.3	3.55
B9	259.8	2.58
B10	-2.2	2.30
B11	-10.9	1.25

Table 2: The precise values of elevation change in meters given over the appropriate B-zone. Area of B-zones are given in squared meters. These values correspond to figures 3 and 4.

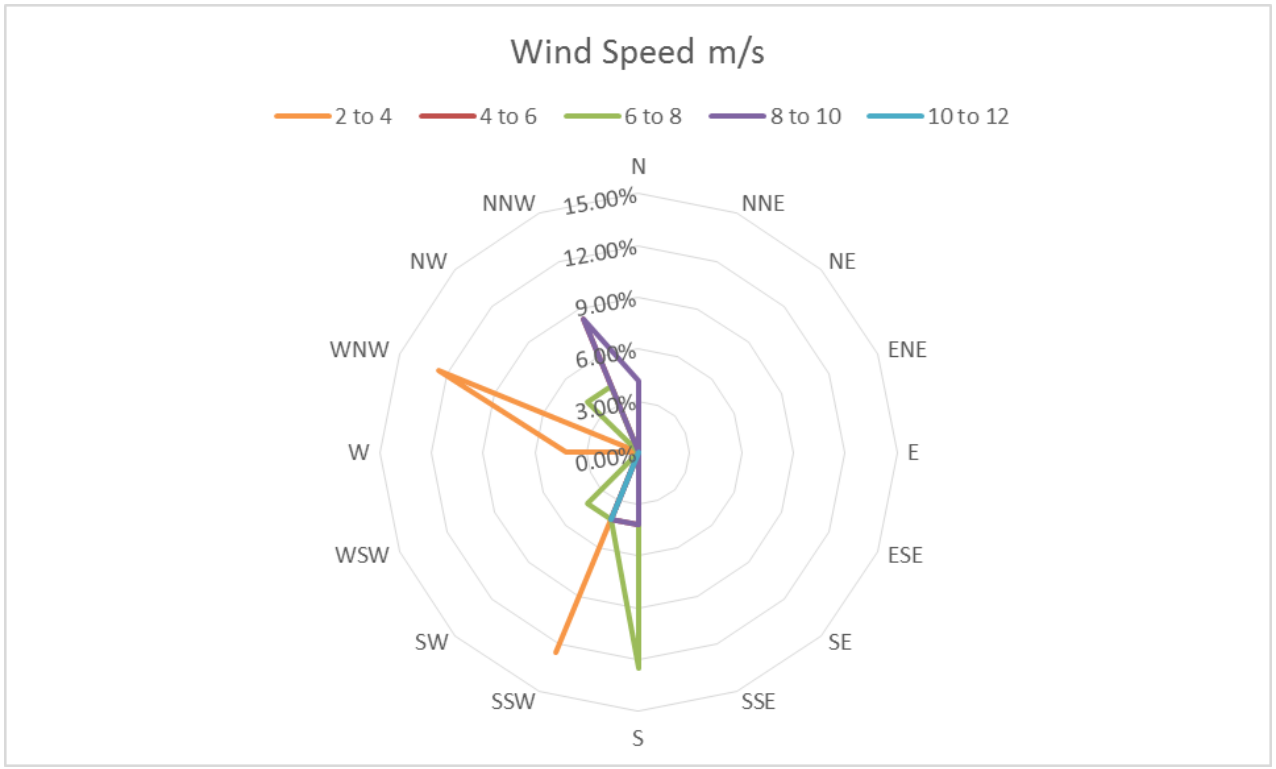

Figure 5. This wind rose shows the wind directions taken in six-hour intervals from 7 November 2015 to 12 November 2015 in terms of percentages. All data for this wind rose was collected using online archives (timeanddate.com). Color-coded wind-speed ranges given in m/s are provided for by the legend. The extent that each wind-velocity petal reaches out gives an indication of how often wind blew in that particular direction with in that particular velocity range in terms of a percentage. When comparing this plot with trends seen in figures 1 and 3, it can be seen that regions of sediment deposition/accumulation correspond to prominent wind direction, except for in the case of sediment accumulation occurring in the east. It is worth considering that winds with a velocity within a range from 2 to 4 m/s (orange) might have lack the energy to transport sand-sized grains a significant amount, so sediment transport in a westerly direction may be less prominent than what is initially suggested by the plot. When ignoring winds with velocities less than 6 m/s, it becomes clear that southerly winds and northerly winds were dominant, and it is in these direction that sediments were most accumulated.

Average Elevation Change (mm):	-4.16
Average Volumetic Change (mm^3):	-137.63
Average Wind Velocity (m/s)	2.17
Average Wind Direction	WSW

Table 3. The total average elevation change, volumetric change, and wind parameters from 7 November 2015 to 12 November 2015. There was an overall decrease in the average dune elevation, and thus an average decrease in the average volume of sediment on the dune. It is important to note that this average volumetric change did not take into account an increase in the actual dune area, and was calculated simply by multiplying average elevation change by the area from which the average elevation change was taken from.

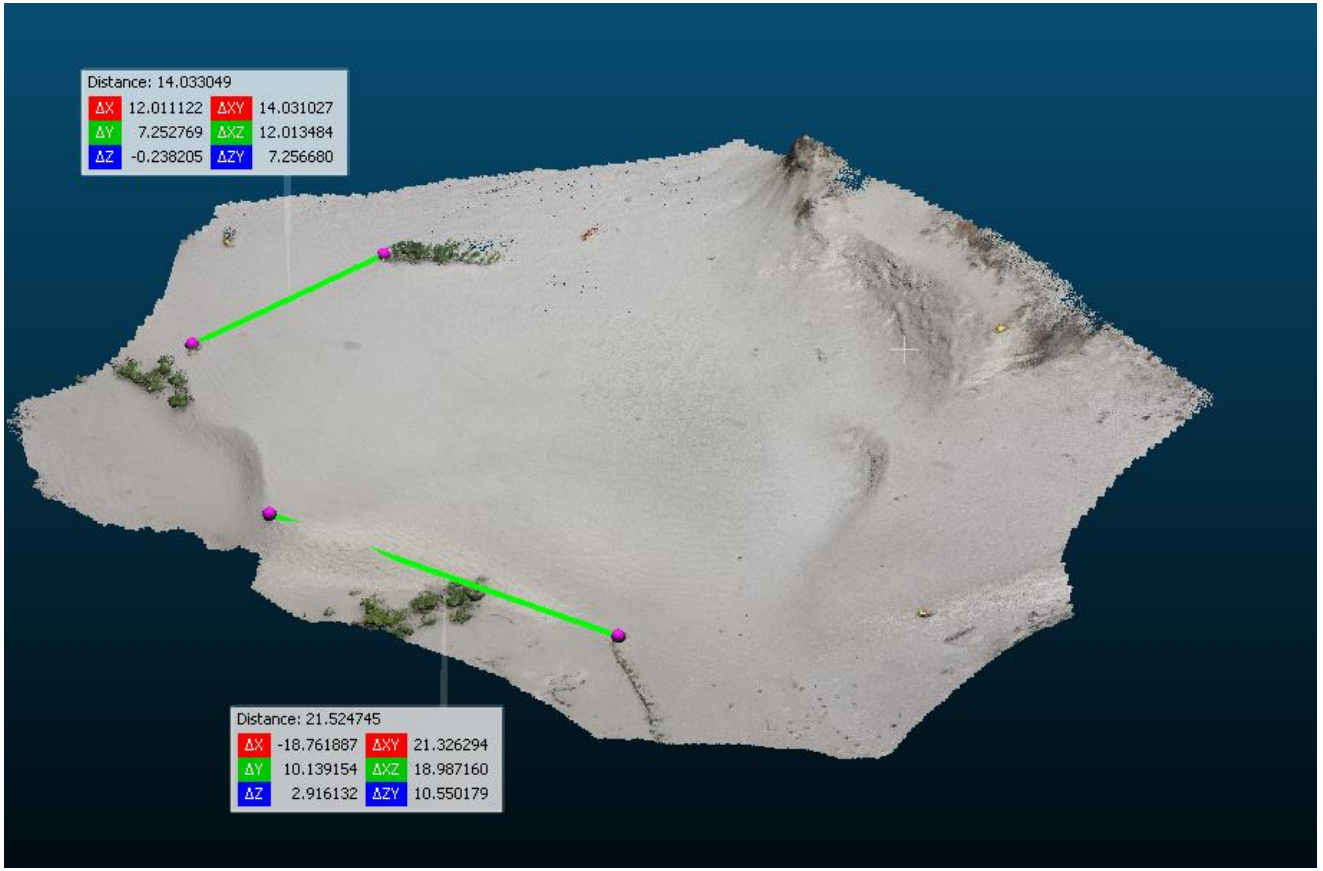

Figure 6. An image of the point cloud generated from photos taken on 7 November 2015. One of the lines shown in the image played an important role in the establishment of real world units for the DEMs. Vegetation patches and topographic features can be easily seen.

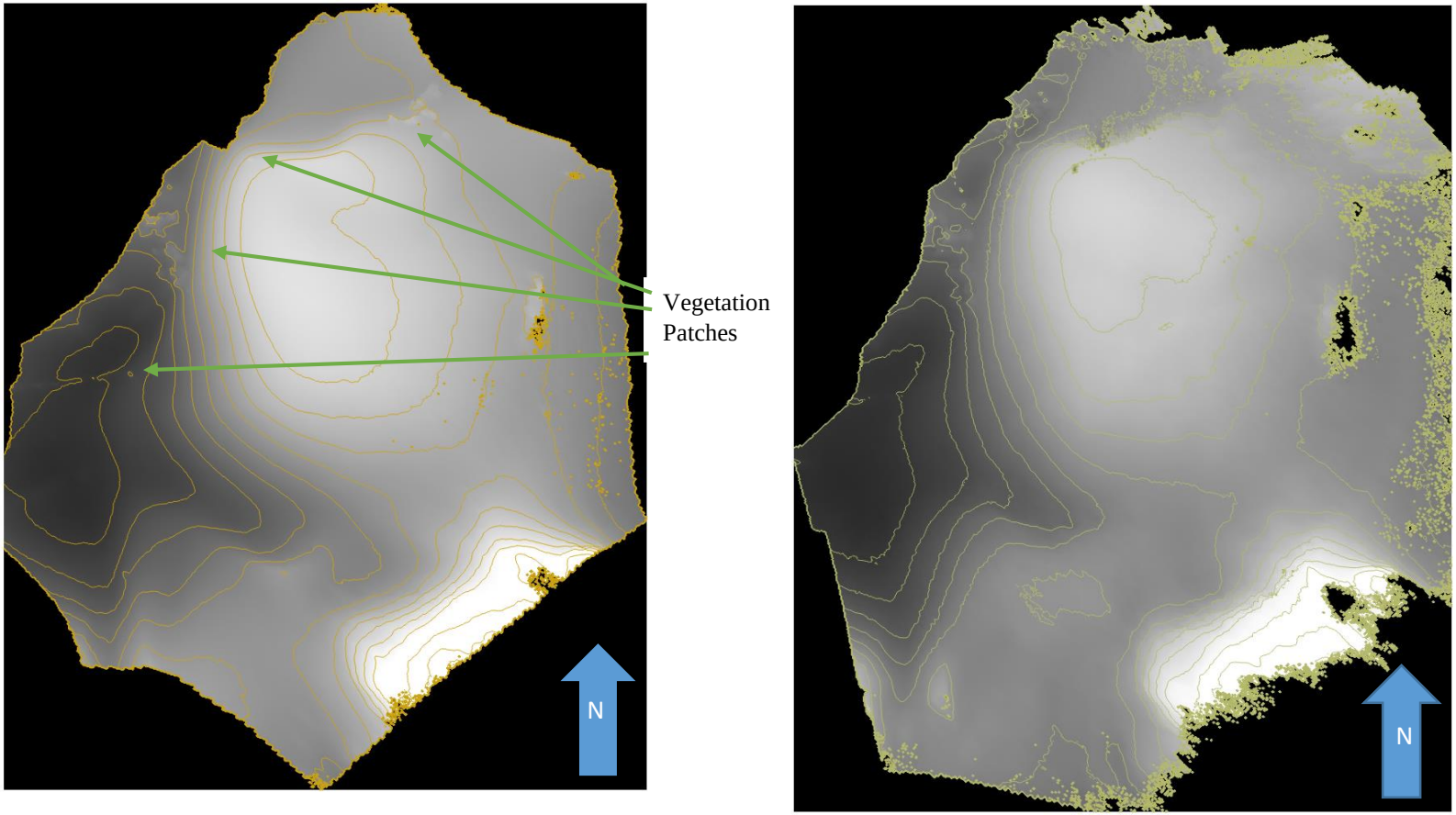

Figures 7 & 8. The left image is the scaled DEM representing the height values for the dune on 7 November 2015. The right image is the scaled DEM representing the height values for the dune on 12 November 2015. The contour interval in the two images roughly corresponds to 10 cm. These point-cloud derived DEMs are fine enough so that one may distinguish features such as vegetation patches. This level of precision was important for purposes of aligning the point clouds, as well as scaling the DEMs to real-world scale, as these procedures required the selection of distinguishable points with real-world measurements associated with them. Even without subtracting the two DEMs, differences in the micro topography can be seen with decent level of detail. Just off of the bottom-left (south-east) region of the screen is an elevated ridge-like region of the dune that was parallel to the shoreline.

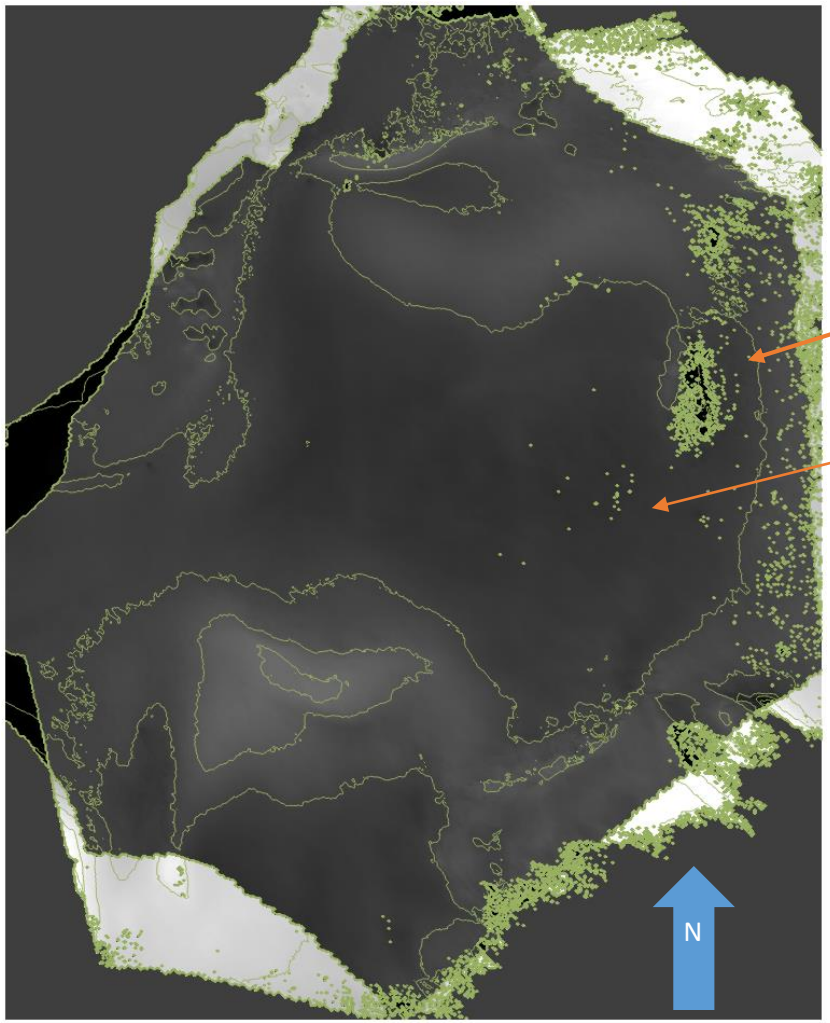

Figure 9. The raster obtained by subtracting the 9 November 2015 DEM from the 12 November 2015 DEM after alignment and scaling. The values from this raster were used in the statistical analysis and interpretation for the report. Brighter regions correspond to areas where sediment was accumulated, while darker regions corresponded to areas where sediment was removed. The contour interval is roughly 10 centimeters and further highlight regions where elevation change occurred. The edges and regions adjacent to plant matter were not covered by the polygonised zones in figures 1 and 3, so no data for these regions was collected. Small bright spots where zones B8 & B9 cover can be seen, these small bright spots provide potential sources of error which the certainly skew the sediment change upwards in the zones they are located in. The cause of these bright spots is most likely a lack of points associated with the second point-cloud in those spots. Large brighter bands can be seen in the northern and southern regions, which, when taking figure 5 into account, provides evidence for sediment being deposited and overall accumulating in regions downwind the brief period between photo acquisition.

References:

M.J. Westoby, J. Brasington, N.F. Glasser, M.J. Hambrey, J.M. Reynolds. ‘Structure-from-Motion’ photogrammetry: a low-cost effective tool for geoscience applications. Geomorphology, 179 (2012), pp. 300-314.

S.L Forman, L. Nordt, J. Gomez, J. Pierson. Late Holocene dune migration on the south Texas sand sheet. Geomorphology, 108 (2009), pp. 159-170.